Modular Synthesis of Templated Bimetallic Sites in Metal-Organic Framework Pores

Jackson Geary, a Jonathan P. Aalto, and Dianne J. Xiaoa,*

^aDepartment of Chemistry, University of Washington, Seattle, Washington 98195-1700, United States.

*Corresponding author: djxiao@uw.edu

ABSTRACT: Binuclear metal active sites are found throughout all subfields of catalysis, from homogeneous and heterogeneous systems to enzymes. Here, we report a synthetic route to install well-defined bimetallic sites in metal—organic frameworks that offers independent control over the ligand environment, metal identity, metal—metal distance, and pore environment. Our approach uses thermolabile tertiary carbamate crosslinkers to template pairs of amine functional groups within framework pores. The templated amine pairs can be quantitatively converted into diverse chelating sites, such as iminopyridine and bis(2-pyridylmethyl)amine ligands, and metalated with a variety of metal cations (M = Mn(II), Fe(II), Co(II), Ni(II), Cu(I), and Cu(II)). A combination of density functional theory, extended X-ray absorption fine structure spectroscopy, and electron paramagnetic resonance spectroscopy is used to confirm the local coordination environment and support the proximal nature of the templated bimetallic sites. The templating strategy described here will enable the exploration of new bimetallic motifs in heterogeneous catalysis.

Introduction.

Enzymes often use two or more metal sites to catalyze difficult oxidative, reductive, and redox-neutral transformations. For example, nature uses diiron and dicopper sites to activate O₂ and oxygenate substrates, ^{1,2} as well as diiron and [NiFe] centers to reversibly form and split H₂.^{3,4} Two metal cations can also work jointly to increase the electrophilicity and nucleophilicity of reaction partners, such as in the hydrolysis of phosphate ester and amide bonds.^{5,6} We have been interested in translating these bioinspired concepts to a heterogeneous platform, to leverage the greater stability, recyclability, and unique microenvironments found in porous materials.

An ideal heterogeneous scaffold would, like enzymes, offer precise control over the active site nuclearity and metal-metal distance, as well as the identity and flexibility of the primary coordination sphere. These complex structural requirements represent an exciting opportunity for metal-organic frameworks (MOFs), a class of porous materials characterized by high structural and chemical tunability. Multiple strategies to install homo- and heterobinuclear metal active sites on MOF surfaces have been reported, and these prior examples can be roughly divided into two categories. In the first approach, multinuclear metal nodes are used directly as the catalytic centers. Coordinatively unsaturated binuclear metal nodes can be used without further modification, while larger nuclearity nodes, such as 1D chains, must be converted into site-isolated bimetallic sites through the synthesis of mixed-metal variants.8 In the second approach, bimetallic active sites are postsynthetically grafted onto the pore walls. Reactive surface hydroxyl sites. 9-11 Lewis acidic metal cations, 12 or organic functional groups on the ligand struts^{13,14} have all been used as the points of attachment. However, in the absence of pre-formed clusters^{9,13} or highly constrained binding pockets, ¹¹ complex metal speciation is often observed in both approaches.

Grafting bimetallic active sites to MOFs via covalent attachment to the ligand strut is a particularly appealing approach (**Fig. 1**), as it not only provides a robust connection to the framework surface but can also be adapted to diverse ligand environments, metal precursors, and pore structures. For example, amine-functionalized frameworks have been used to attach salicylidene, is iminopyridine, ind NNN-pincer complexes to pore walls, as well as iminocatecholate-bound Ru(II) metathesis catalysts (**Fig. 1a**). Furthermore, amine groups are readily

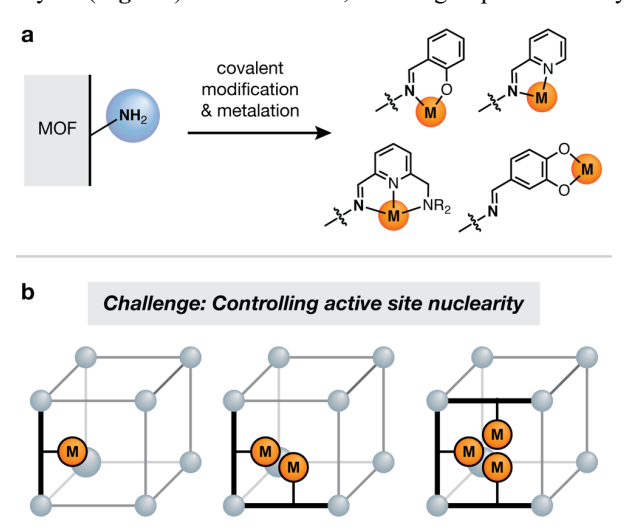
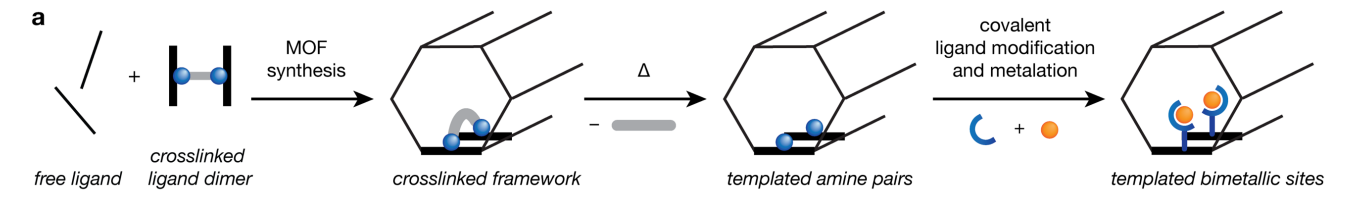


Figure 1. (a) Previously reported strategies to graft metal complexes onto amine-functionalized metal—organic frameworks. The free amine group can be covalently modified and converted into chelating ligands. (b) Adapting covalent grafting strategies to the construction of binuclear metal active sites introduces new challenges, such as controlling active site nuclearity.



tunable active site density, M-M distance, & pore structure

tunable ligand environment & metal identity

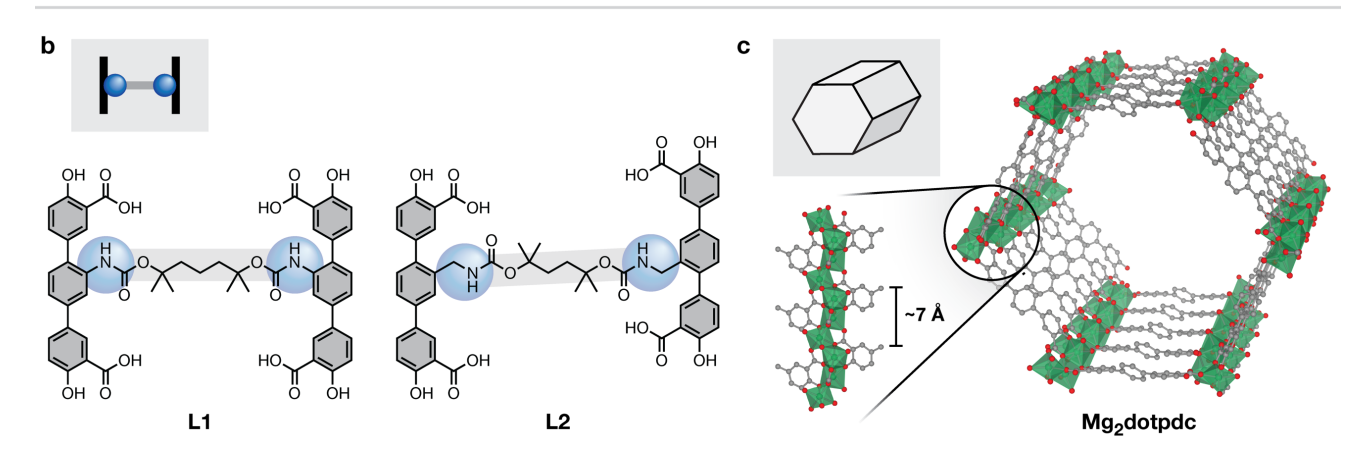


Figure 2. (a) Overview of the templating strategy employed in this work, which leverages thermolabile crosslinkers to install pairwise bimetallic active sites. (b) Structures and abbreviations of ligands and crosslinked ligand dimers used in this work. L1 and L2 contain N-aryl and N-alkylcarbamate linkages, respectively. (c) Structure of Mg_2 dotpdc, a mesoporous MOF which possesses an interligand spacing of \sim 7 Å down the hexagonal pore channels.

incorporated into many common MOF structure types.²⁰ However, while postsynthetic covalent grafting offers a large selection of possible ligand and pore environments, an unresolved challenge is controlling the active site nuclearity. Grafting at low surface coverages results in predominantly mononuclear sites, while higher loadings risk the formation of larger nuclearity clusters (**Fig. 1b**).

Here, we describe a templating approach to circumvent these challenges and install well-defined binuclear metal active sites in framework pores, irrespective of the active site density (**Fig. 2**). Thermolabile tertiary carbamate crosslinkers are used to tether pairs of amine functional groups during framework synthesis. Postsynthetic crosslinker cleavage reveals templated aryl- and alkylamines that can be used to graft atomically precise bimetallic iminopyridine and bis(2-pyridylmethyl)amine complexes with a variety of metals (e.g., Mn(II), Fe(II), Co(II), Ni(II), Cu(I), and Cu(II)). The structural integrity of the frameworks is confirmed by powder X-ray diffraction and gas sorption measurements, while the local structure of the metal centers is probed by density functional theory (DFT), extended X-ray absorption fine structure (EXAFS) spectroscopy, and electron paramagnetic resonance (EPR) spectroscopy.

Results and discussion.

Synthesis of templated amine-functionalized frameworks.

We recently showed that cleavable covalent crosslinkers can be used to template functional group pairs in multicomponent metal—organic frameworks.²¹ Specifically, thermolabile tertiary ester crosslinkers can be used to install well-defined carboxylic acid pairs within the terphenyl-expanded MOF-74 framework, also known as Mg_2 dotpdc (dotpdc⁴⁻ = 4,4"-dioxido-[1,1':4',1"-terphenyl]-3,3"-dicarboxylate). When short pentyl crosslinkers

are used, modeling studies showed that the carboxylic acids are installed in a single configuration down the pore channels, spaced \sim 7 Å apart.

Given the thermal instability of tertiary carbamates, ²² we hypothesized that a similar strategy could be used to template pairs of amines within framework pores (**Fig. 2a**). Amines are ideal entry points to more complex structures thanks to their rich postsynthetic chemistry. ²³ They have been shown to undergo a multitude of reactions within MOF pores, including imine formation, ¹⁶ urea formation, ^{24,25} alkylation, ²⁶ and acylation. ²⁷ In principle, it should be possible to convert templated amine pairs into diverse site-isolated bimetallic sites via established postsynthetic ligand modification and metalation steps.

Towards this goal, we synthesized two distinct crosslinked ligand dimers, each containing thermolabile tertiary carbamate linkages (**Fig. 2b**). The lengths of both crosslinkers were designed to span the short ~7 Å interligand distance down the pore channel of Mg₂dotpdc (**Fig. 2c**). The ligand dimer **L1** is constructed from *N*-aryl carbamate linkages, which should produce arylamines after thermolysis. In contrast, **L2** contains *N*-alkylcarbamate linkages, which should template more nucleophilic alkylamine pairs. Both ligand dimers were synthesized in 4–5 steps in good overall yield (42–60%, see SI for experimental details).

With spatially separated, site-isolated bimetallic pairs in mind, we targeted the synthesis of carbamate-crosslinked Mg₂dotpdc at relatively low crosslinker loadings (<20 mol%). Heating a mixture of crosslinked ligand dimer (0.100 equiv), H₄dotpdc (0.900 equiv), and Mg(NO₃)₂•6H₂O (2.75 equiv) in a solution of DMF and MeOH produced microcrystalline powders with the desired Mg₂dotpdc structure. Keeping in mind that

each equivalent of L1 or L2 contains two ligand monomers, this reaction mixture should theoretically lead to ~18% functional group loading. The exact composition of the framework was quantified by digestion ¹H NMR (Table S1). Consistent with previous work,²¹ the experimentally observed incorporation of **L1** or **L2** varied slightly, but was typically slightly higher than the value expected based on the initial ratio of starting materials. Using the ligand dimer L1, we obtained a framework containing 18% crosslinked (i.e., functionalized) ligand, which we have abbreviated as 1-XL-18% (Fig. S3). Similarly, using the ligand dimer L2 under these conditions produced a material containing 23% crosslinked ligand, which we have abbreviated 2-XL-23% (Fig. S4). Both chemically crosslinked frameworks are permanently porous, displaying high Brunauer-Emmett-Teller (BET) surface areas of 2370 m²/g and 2400 m²/g for 1-XL-18% and 2-XL-23%, respectively (Fig. S5).

Due to the short length of the crosslinking tether, the ligand monomers in L1 and L2 should lie directly adjacent down the pore channels (Fig. 2a). DFT modeling studies suggest that the conformation shown in Fig. 3a, where the amine groups are oriented in the same direction rather than offset, is most favorable for both dimers (Fig. S6 and Table S2, see SI for additional modeling details).

With the desired crosslinked frameworks in hand, we next sought to cleave the carbamate linkage and reveal exposed amine pairs. The thermal cleavage of tertiary carbamates has been successfully demonstrated not only in simple organic compounds²² but also in solid-state porous materials including silica^{28,29} and metal–organic frameworks.^{30–32} Thermogravimetric analyses confirmed the thermal lability of the crosslinkers (Fig. S7-S8). Excitingly, subjecting 1-XL-18% to microwave heating at 230 °C in a mixture of 2-ethyl-1-hexanol and ethylene glycol for 10 minutes resulted in quantitative carbamate cleavage and formation of 1-NH2-18%, a framework containing templated arylamines (Fig. 3a). No loss in crystallinity was detected by powder X-ray diffraction (PXRD) (Fig. 3b), and a large increase in the BET surface area from 2370 m²/g to 2650 m²/g was observed (Fig. S9). This value is very close to the reported surface area for unfunctionalized Mg₂dotpdc (~2700 m²/g).²¹ Full crosslinker removal was further confirmed by digestion ¹H NMR. No peaks associated with the crosslinker could be detected, and the amount of H₄dotpdc-NH₂ found was consistent with the starting amount of L1 (Fig. S8).

The carbamates in **2-XL-23%** could be cleaved using either microwave heating under air-free conditions, or conventional heating in the solid state under flowing N₂. Similar conditions have been previously used to remove tert-butoxycarbonyl (Boc) protecting groups in MOFs.³² Heating samples of **2-XL-23%** at 250 °C for two days under flowing N₂ resulted in clean conversion to **2-CH₂NH₂-23%**. Like **1-NH₂-18%**, no loss in crystallinity was observed (**Fig. 3b**), and the BET surface area increased from 2400 m²/g to 2610 m²/g (**Fig. S11**). Digestion ¹H NMR analysis confirmed quantitative crosslinker removal and the clean conversion of **L2** to two equivalents of H₄dotpdc-CH₂NH₂ (**Fig. S12**).

Postsynthetic imine formation and metalation. The ability to template amine pairs in MOF pores provides the opportunity to create bimetallic active sites where all structural parameters, from the ligand environment and metal identity to the metalmetal distances and pore environment, can be carefully controlled (**Fig. 2a**). Motivated by the widespread use of iminopyridine ligands in organometallic chemistry, ^{33–35} we

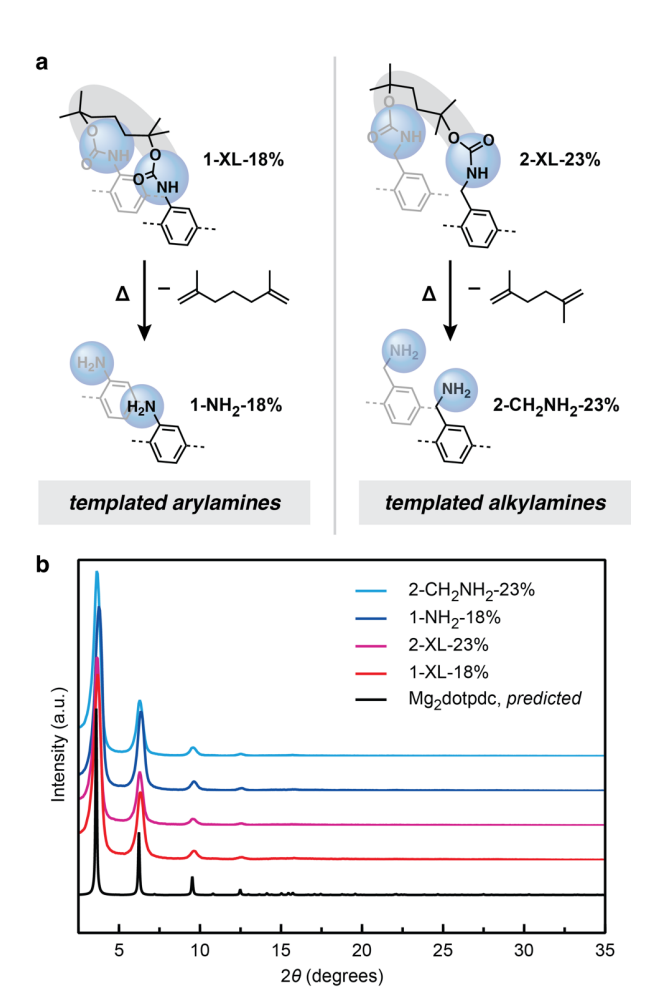


Figure 3. (a) Overview of thermolysis conditions to generate templated arylamine and alkylamine pairs. Powder X-ray diffraction data (b) and 77 K nitrogen adsorption data (c) for the crosslinked materials 1-XL-18% and 2-XL-23%, and the thermolyzed frameworks 1-NH₂-18% and 2-CH₂NH₂-23%.

envisioned that the templated arylamines in 1-NH₂-18% could be converted into bimetallic iminopyridine complexes (Fig. 4a).

Iminopyridine formation and metalation in MOFs has been previously demonstrated by several groups, ^{16,17,36,37} and both stepwise and one-pot synthetic approaches have been explored. In the stepwise approach, excess 2-pyridinecarboxaldehyde (PyCHO) is first added to the amine-functionalized framework to form discrete MOF-supported iminopyridine sites, which are subsequently metalated in a second step. ^{16,37} In the one-pot approach, excess PyCHO and metal halide salt (e.g., NiCl₂) are combined together to form a molecular (PyCHO)MX₂ complex, which is then combined with the framework to form the desired metalated iminopyridine species. ^{17,36}

We first tested the one-pot condensation and metalation of **1-NH**₂ with 10 equiv of 2-pyridinecarboxaldehyde and metal salt (NiCl₂ or CuCl) in methanol. Excitingly, we observed near-quantitative conversion of **1-NH**₂ to **1-(IP)M** (M = NiCl₂, CuCl), a framework containing surface-supported bimetallic metal iminopyridine complexes (90% yield for NiCl₂ and 100% for CuCl) (**Table S3, Table 1**). Successful iminopyridine formation and metalation were quantified by ¹H NMR and ICP analysis of digested frameworks, respectively (**Table S3**). Both crystallinity and surface area were maintained in the metalated

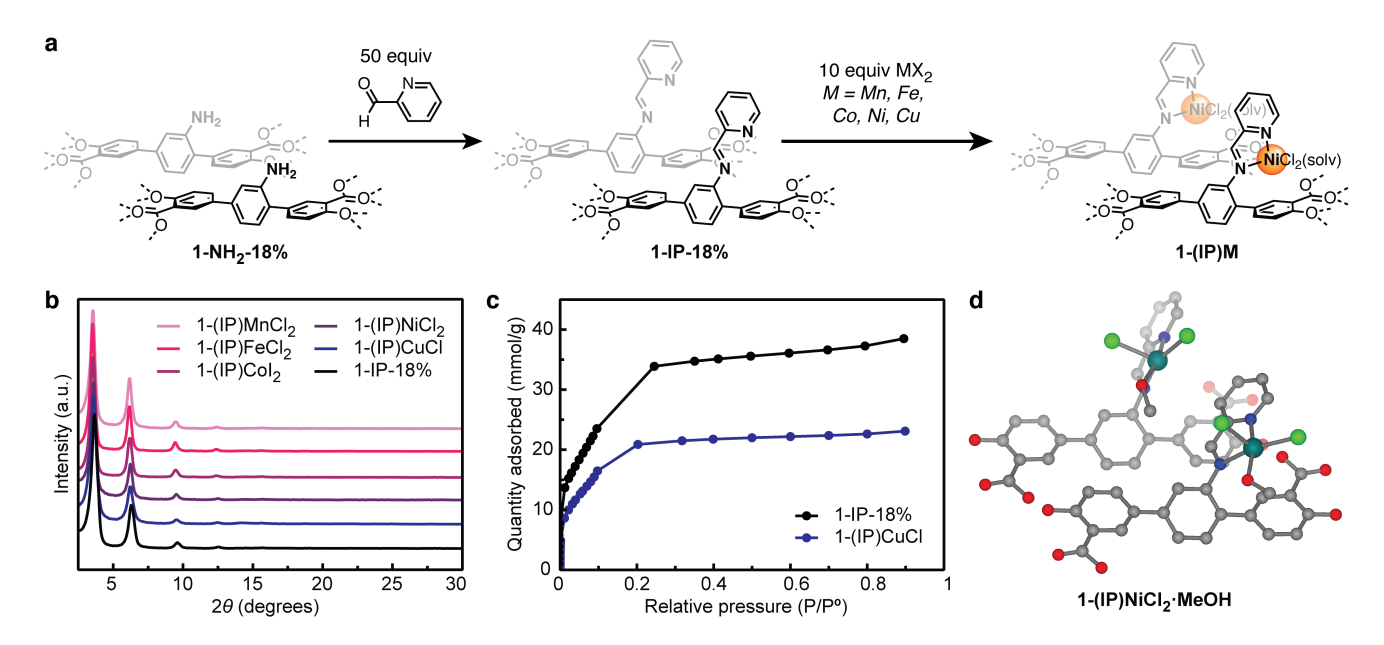


Figure 4. (a) Overview of the stepwise route to generate 1-(IP)M from 1-NH₂-18%. Powder X-ray diffraction data (b) and 77 K nitrogen adsorption data (c) for postsynthetically modified 1-IP-18%, and metalated 1-(IP)M. (d) Optimized structure for the metal sites in 1-(IP)NiCl₂·MeOH obtained via DFT using a split B3LYP/6-31+G(d), B3LYP/LANL2DZ basis set. Additional ligand layers omitted for clarity.

frameworks (**Fig. 4b**), and a BET surface area of 1700 m²/g was observed for **1-(IP)CuCl (Fig. 4c**).

While the one-pot approach worked well for Ni(II) and Cu(I), generalizing this strategy to other metal cations was challenging due to the precipitation of insoluble PyCHO-containing metal species. 38,39 In an effort to expand our metalation catalogue, we returned to the stepwise route. Initial attempts to form iminopyridine species in the absence of Lewis acidic transition metal salts yielded poor conversion to the imine (e.g., <50% yield after 7 days). 16 Surprisingly, simply switching from the nonpolar solvents commonly used in the MOF literature (e.g., DCM, toluene) to a more polar solvent such as methanol greatly improved the yield. Heating 1-NH₂-18% in methanol with a large excess of 2-pyridinecarboxaldehyde (50 equiv) resulted in the clean formation of 1-IP-18%, with a BET surface area of 2450 m²/g (**Fig. 4c**). The reaction could be tracked by digestion ¹H NMR. Though the digestion conditions hydrolyze the imine, the observed 1:1 ratio of 2-pyridinecarboxaldehyde to H₄dotpdc-NH₂ is consistent with quantitative imine formation (**Fig. S13**). The loss of the broad amine N–H stretch is clearly observed in the ATR-FTIR spectra, further supporting the conversion of the amine to the imine (Fig. S14).

With the iminopyridine-functionalized framework in hand, metalation proceeded smoothly with a variety of M(I) and M(II) salts (e.g., MnCl₂, FeCl₂, CoI₂, NiCl₂, NiBr₂, CuCl) to generate **1-(IP)M-18%** (**Table 1**). The crystallinity of the metalated materials was confirmed by PXRD (**Fig. 4b**), and metalation was quantified by ICP analysis (**Table S3**). While nearly all transition metals tested led to >90% metalation, a notable exception was Cu(II), which leached in acetonitrile and formed side products in methanol. Overall, this work establishes a remarkably general route to achieve bimetallic iminopyridine species with diverse metal cations.

Postsynthetic alkylation and metalation. Given the increased nucleophilicity and flexibility of alkylamines, we hypothesized that new MOF-supported multidentate ligand

scaffolds could be accessed through S_N2 alkylation of 2- CH_2NH_2 -23% (Fig. 5). In particular, alkylation is a common way to achieve polypyridyl ligand scaffolds. For example, double alkylation of the amine sites in 2- CH_2NH_2 -23% with 2-(bromomethyl)pyridine should generate tridentate bis(2-pyridylmethyl)amine ligands, also commonly known as di-(2-picolyl)amine (DPA) (Fig. 5a). While polypyridylamine ligands are found throughout inorganic chemistry, particularly in the study of biomimetic dicopper and diiron—oxo and dioxygen chemistry, 40,41 to our knowledge no polypyridylamine complexes have been previously grafted in a metal—organic framework.

Table 1. Metalations summary as determined by ICP-OES.

Framework	Metal Identity	Metalation Yield (%)
1-IP-18%	MnCl ₂ ^b	100
	FeCl ₂ ^b	100
	CoI_2^b	89
	NiBr ₂ ^b	89
	CuCl ^a	100
2-DPA-23%	$FeCl_2$	100
	CoI_2	100
	$NiBr_2$	83
	$CuBr_2$	100
2-DPA-5%	$CuCl_2$	100
	Cu(OTf) ₂	100

^a Synthesized using the one-pot method.

Gratifyingly, double alkylation of the alkylamine sites in 2- CH_2NH_2 -23% with 2-(bromomethyl)pyridine hydrobromide

^b Synthesized using the stepwise method.

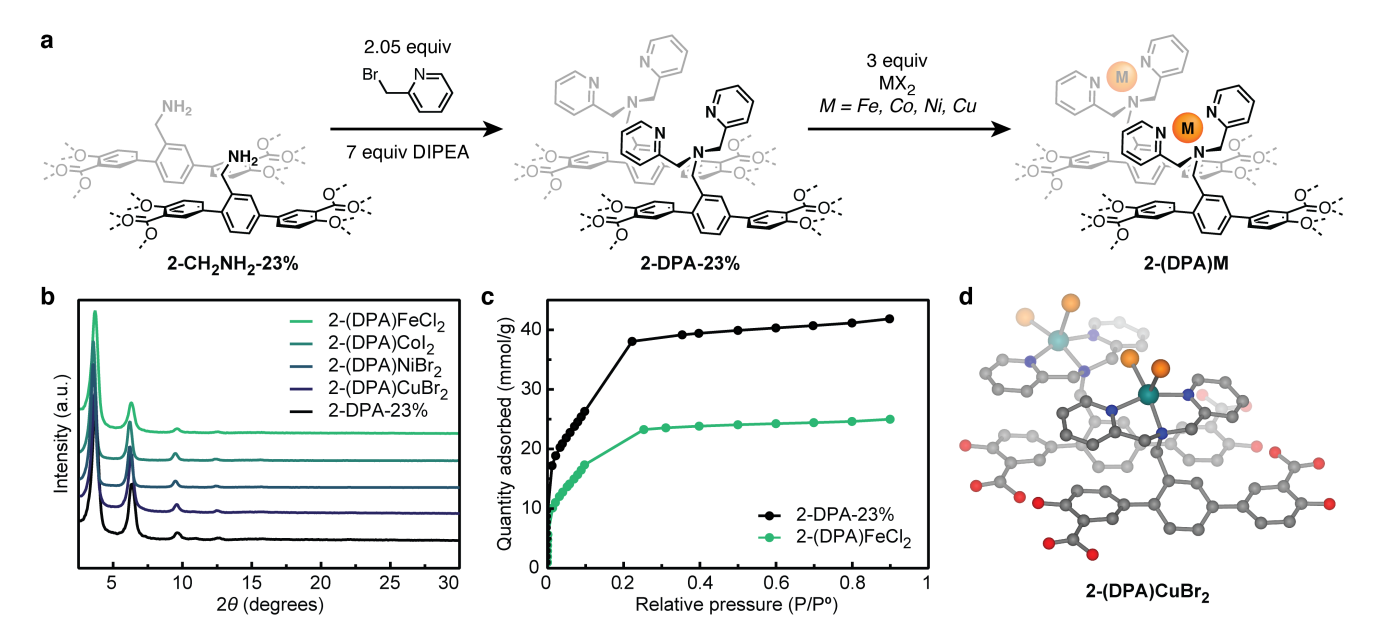


Figure 5. Overview of postsynthetic reactions to generate **2-(DPA)M** from **2-CH₂NH₂-23%**. Powder X-ray diffraction data (b) and 77 K nitrogen adsorption data (c) for postsynthetically modified **2-DPA-23%**, and metalated **2-(DPA)M**. (d) Optimized structure for the metal sites in **2-(DPA)CuBr₂** obtained via DFT using a split B3LYP/6-31+G(d), B3LYP/LANL2DZ basis set. Additional ligand layers omitted for clarity.

proceeded smoothly in the presence of diisopropylethylamine in acetonitrile. The ¹H NMR spectrum of the digested framework shows the appearance of diagnostic pyridyl and methylene peaks, along with the complete disappearance of signals corresponding to the unalkylated benzylamine ligand, H₄dotpdc-CH₂NH₂ (**Fig. S15**). The resultant material, abbreviated **2-DPA-23%**, is readily metalated with a number of first row transition metals (M = Fe(II), Co(II), Ni(II), and Cu(II), see **Table 1**) in 90–100% yield. Both **2-DPA-23%** and the metalated materials retain crystallinity and porosity (**Fig. 5b**), with **2-DPA-23%** possessing a BET surface area of 2540 m²/g and **2-(DPA)FeCl₂** possessing a BET surface area of 1760 m²/g (**Fig. 5c**).

Spectroscopic characterization of bimetallic sites. We next carried out a combination of extended X-ray absorption fine structure (EXAFS), density functional theory (DFT), and electron paramagnetic resonance (EPR) studies to structurally interrogate the metal sites in 1-(IP)M and 2-(DPA)M. Two air-stable materials, 1-(IP)NiCl₂ and 2-(DPA)CuX₂ (X =Br, OSO₂CF₃), were selected as representative frameworks for these studies.

Excitingly, EXAFS studies on both frameworks confirm that the MOF-supported metal sites reside in well-defined ligand environments that closely resemble their molecular counterparts. The Ni K-edge EXAFS spectrum of 1-(IP)NiCl₂ is shown in Fig. S16. The EXAFS data was best fit with three N/O atoms at a distance of 2.03(6) Å and two Cl atoms at 2.29(7) Å (Table S4). The presence of an additional ligand is expected, as coordinating methanol is used in the metalation and washing procedure. These bond distances are consistent with the DFT optimized structure for 1-(IP)NiCl₂ (Fig. 4d, Table S5), as well as with previously reported five-coordinate nickel(II) iminopyridine complexes, which show average Ni–N/O and Ni–Cl distances of ~2.0–2.1 Å and ~2.3 Å, respectively (see Table S6 for a tabulation of reference compounds).

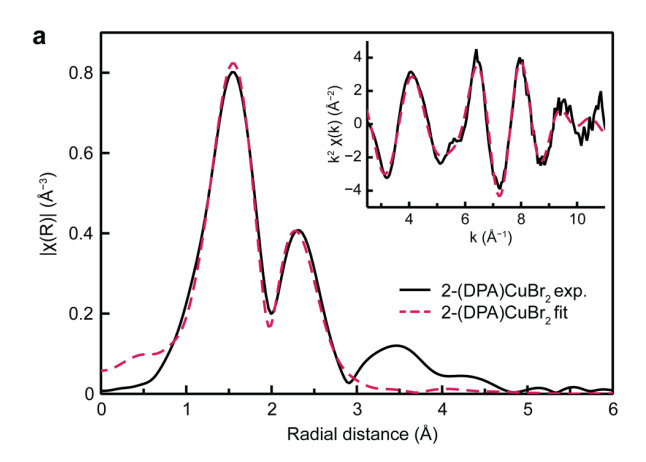
The Cu K-edge EXAFS spectrum of **2-(DPA)CuBr**₂, shown in **Fig. 6a**, was best fit with two pyridyl N atoms at 2.01(1) Å, one alkyl N atom at 2.14(1) Å, one Br atom at 2.40(1) Å, and a second Br atom at 2.79(1) Å (**Table S7**). This is consistent with previously reported bis(2-pyridylmethyl)amine-ligated Cu(II) molecular complexes, which often adopt distorted square pyramidal geometries featuring one shorter basal Cu–Br bond (~2.40 Å) and one significantly longer apical Cu–Br bond (~2.70 Å) (see **Table S8** for tabulation of reference compounds). The bond lengths observed by EXAFS are also consistent with DFT-optimized structural models (**Fig. 5d** and **Table S9**).

Notably, no evidence of strong M–M scattering was observed in any of the EXAFS spectra. Indeed, the EXAFS spectra of templated frameworks and their non-templated analogues are nearly identical (**Fig. S17, S18**). Given the \sim 7 Å distance between ligand struts and the lack of strong bridging ligands between the two metal centers, the M–M distances are likely beyond the \sim 4–5 Å distance detectable by EXAFS. Therefore, we turned to EPR spectroscopy as a more sensitive probe of proximal paramagnetic centers.

Electron paramagnetic resonance spectroscopy is highly sensitive to the interactions between unpaired electrons, and is widely used to probe interspin distances. A2,43 These interactions may be either exchange (through orbital overlap) or dipolar (through space) interactions. Given the expected $\sim 7 \, \text{Å}$ distance between our metal centers by DFT, the lack of short M–M distances observed in our EXAFS data, and the absence of strong bridging ligands, we only expect spin-spin interactions through dipolar coupling. Because our templated frameworks have shorter average M–M distances than non-templated controls, this should lead to two distinct differences: 1) the EPR features for the templated samples should show greater homogeneous line broadening, and 2) the relative intensity of the forbidden $\Delta m_s = 2$ half-field transition should increase.

To simplify the analysis, all EPR studies were carried out on **2-(DPA)Cu(OTf)**₂, an $S = \frac{1}{2}$ system. Due to the high sensitivity of EPR towards dipolar interactions, low amine loadings of 5% were targeted. Two frameworks were synthesized, the templated framework **2-(DPA)Cu(OTf)**₂-**5%** and the non-templated control, Mg₂dotpdc-(DPA)Cu(OTf)₂-**5%**. Briefly, the non-templated framework was synthesized using H₄dotpdc-CH₂NHBoc, a non-crosslinked ligand containing Boc-protected benzylamine groups. The protected framework was then subjected to thermolysis, post-synthetic alkylation, and metalation to yield randomly distributed mononuclear (DPA)Cu(OTf)₂ sites throughout the framework (see SI for more experimental details).

Unexpectedly, a sharp isotropic feature at g = 2.002 was observed in all thermolyzed samples. We assign this feature to a ligand-based organic radical generated during the thermal deprotection step, as it is observed even in the unfunctionalized Mg₂dotpdc after thermal treatment (**Fig. S19**). We note that careful air-free thermolysis under microwave conditions minimizes, but does not fully eliminate, the presence of this radical species, suggesting it arises due to oxidation of the framework backbone at high temperatures.



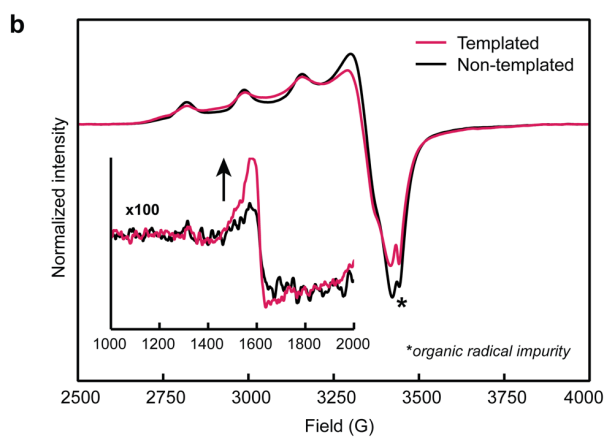


Figure 6. (a) Fit (red dashed lines) to EXAFs spectrum of **2-(DPA)CuBr₂** (solid black line). (Inset) Corresponding k^2 -weighted oscillations. See SI for fit parameters. (b) 100K X-band EPR spectra for **2-(DPA)Cu(OTf)₂** and the non-templated control framework, Mg₂dotpdc-DPA-Cu(OTf)₂. The forbidden $\Delta m_s = 2$ transition at 100x magnification is shown in the inset. The framework organic radical that appears after thermolysis is marked with an asterisk.

The X-band EPR spectra of the templated **2-(DPA)Cu(OTf)₂-5%** and the non-templated Mg₂dotpdc-(DPA)Cu(OTf)₂-5% control were collected at 100 K and analyzed (**Fig. 6b**). The Cu(II) features in both spectra are best fit using two distinct *g*-values (2.06 and 2.24, see **Fig. S20–S21**). Similar values have been observed in molecular (DPA)Cu(OTf)₂ complexes. 46,47 To control for slight variations in copper loading between the samples, both spectra were normalized to the double integral of the allowed $\Delta m_s = 1$ transition.

Excitingly, both greater line broadening as well as an increase in the intensity of the forbidden transition at $g \sim 4$ is observed in **2-(DPA)Cu(OTf)₂-5%** relative to the non-templated analogue (**Fig. 6b** and **Table S10**). While subtle, this data provides evidence that the templated framework has shorter average M–M distances. Greater differences in both the EPR and EXAFS data and more quantitative analysis should be possible with the addition of bridging ligands to tether the two metal sites closer together (<4 Å), and work along this vein is underway.

Conclusion.

In summary, we have developed a strategy to precisely template pairs of aryl- and alkylamines in a mesoporous metal–organic framework. The templated amines can be further elaborated to achieve atomically precise bimetallic active sites with tunable ligand environments. The iminopyridine and bis(2-pyridylmethyl)amine ligand scaffolds illustrated here have a rich history in organometallic and bioinorganic chemistry, as well as the potential to support unusual bimetallic reactivity. For example, dinucleating iminopyridine ligands have been previously explored in the context of olefin polymerization, 48 while dinucleating polypyridyl scaffolds have been studied for bimetallic O₂ activation, 1.2.40,41 anion sensing, 49 and nucleotide hydrolysis. 50

Finally, we note that previous routes to achieve well-defined bimetallic sites in metal–organic frameworks have focused on active sites with highly constrained metal–metal distances. 9,11,13 Our templated sites, which are conformationally flexible, represent a distinct and complementary alternative to the more rigid, static ligand environments described in earlier reports. Overall, the synthetic precision and flexibility of the templating approach described here will allow researchers to re-examine molecular and enzymatic bimetallic motifs in a heterogeneous context, as well uncover new modes of reactivity.

Experimental Methods.

All the ligand syntheses, framework syntheses, and post-synthetic chemistry are described in detail in the Supplementary Information. Powder X-ray diffraction patterns were collected on either a Bruker D8 Discover diffractometer or a Bruker D2 PHASER benchtop diffractometer. Solution phase NMR data were collected on Bruker AV300, AV301, GG500 or NEO500 instruments. FT-IR spectra were collected using a Perkin Elmer Frontier spectrometer equipped with an ATR crystal. N2 adsorption measurements were performed at 77 K on a Micromeritics 3Flex instrument. Thermogravimetric analysis data were collected using a TA Instruments Q Series analyzer. ICP-OES measurements were performed using a Perkin Elmer Optima 8300 Inductively Coupled Plasma Optical Emission Spectrophotometer. EPR spectra were collected on a Bruker EMXNano at 100 K. The EPR spectra were fit using the EasySpin software package for MATLAB.51

XAS measurements were conducted at the Advanced Photon Source at Argonne National Laboratory on beamline 12-BM (4.5 – 20.0 keV) using a Si(111) monochromator. Powder samples were prepared as wafers without any additional grinding and sealed with Kapton tape. Transmission and fluorescence data were collected at room temperature. Specific details regarding data calibration, normalization, and fitting are discussed in the Supplementary Information.

ASSOCIATED CONTENT

Supporting Information

The Supporting Information is available free of charge on the ACS Publications website.

Additional experimental details, synthetic procedures, and characterization data (PDF)

AUTHOR INFORMATION

Corresponding Author

* djxiao@uw.edu.

Author Contributions

The manuscript was written through contributions of all authors. All authors have given approval to the final version of the manuscript.

ACKNOWLEDGMENT

Initial ligand synthesis studies were supported by the donors of ACS Petroleum Research Fund under PRF# 61949-DNI3. Subsequent framework synthesis, post-synthetic modification and metalation were supported by the National Science Foundation (NSF) under Grant No. 2142798 and the David and Lucile Packard Foundation. This research used the beamline 12-BM of the Advanced Photon Source (APS), a U.S. Department of Energy (DOE) Office of Science user facility operated for the DOE Office of Science by Argonne National Laboratory under Contract No. DE-AC02-06CH11357. Part of this work was conducted at the Molecular Analysis Facility, a National Nanotechnology Coordinated Infrastructure (NNCI) site at the University of Washington, which is supported in part by funds from the National Science Foundation (awards NNCI-2025489, NNCI-1542101), the Molecular Engineering & Sciences Institute, and the Clean Energy Institute. In addition, the authors acknowledge the use of facilities and instrumentation supported by the U.S. National Science Foundation through the UW Molecular Engineering Materials Center (MEM-C), a Materials Research Science and Engineering Center (DMR171797). JCG is supported by an NSF graduate research fellowship. We thank Dr. Sungsik Lee for assisting with the collection of synchrotron XAS data at APS beamline 12-BM. We thank the Mary Gates research scholarship for supporting JPA. The NMR facility at the UW Department of Chemistry is supported by NIH Award Number S10OD030224-01A1. This work utilized the computational infrastructure of the Hyak supercomputer system at the UW.

REFERENCES

- Jasniewski, A. J.; Que, L. Dioxygen Activation by Nonheme Diiron Enzymes: Diverse Dioxygen Adducts, High-Valent Intermediates, and Related Model Complexes. *Chem. Rev.* 2018, 118 (5), 2554–2592. https://doi.org/10.1021/acs.chemrev.7b00457.
- (2) Solomon, E. I.; Heppner, D. E.; Johnston, E. M.; Ginsbach, J. W.; Cirera, J.; Qayyum, M.; Kieber-Emmons, M. T.; Kjaergaard, C. H.; Hadt, R. G.; Tian, L. Copper Active Sites in

- Biology. Chem. Rev. **2014**, 114 (7), 3659–3853. https://doi.org/10.1021/cr400327t.
- (3) Fontecilla-Camps, J. C.; Volbeda, A.; Cavazza, C.; Nicolet, Y. Structure/Function Relationships of [NiFe]- and [FeFe]-Hydrogenases. *Chem. Rev.* 2007, 107 (10), 4273–4303. https://doi.org/10.1021/cr050195z.
- (4) Lubitz, W.; Ogata, H.; Rüdiger, O.; Reijerse, E. Hydrogenases. Chem. Rev. 2014, 114 (8), 4081–4148. https://doi.org/10.1021/cr4005814.
- (5) Wilcox, D. E. Binuclear Metallohydrolases. *Chem. Rev.* 1996, 96 (7), 2435–2458. https://doi.org/10.1021/cr950043b.
- (6) Mitić, N.; Smith, S. J.; Neves, A.; Guddat, L. W.; Gahan, L. R.; Schenk, G. The Catalytic Mechanisms of Binuclear Metallohydrolases. *Chem. Rev.* 2006, 106 (8), 3338–3363. https://doi.org/10.1021/cr050318f.
- (7) Wang, C.-H.; Das, A.; Gao, W.-Y.; Powers, D. C. Probing Substrate Diffusion in Interstitial MOF Chemistry with Kinetic Isotope Effects. *Angew. Chem. Int. Ed.* 2018, 57 (14), 3676–3681. https://doi.org/10.1002/anie.201713244.
- (8) Osadchii, D. Y.; Olivos-Suarez, A. I.; Szécsényi, Á.; Li, G.; Nasalevich, M. A.; Dugulan, I. A.; Crespo, P. S.; Hensen, E. J. M.; Veber, S. L.; Fedin, M. V.; Sankar, G.; Pidko, E. A.; Gascon, J. Isolated Fe Sites in Metal Organic Frameworks Catalyze the Direct Conversion of Methane to Methanol. ACS Catalysis 2018, 8 (6), 5542–5548. https://doi.org/10.1021/ACSCATAL.8B00505.
- (9) Desai, S. P.; Malonzo, C. D.; Webber, T.; Duan, J.; Thompson, A. B.; Tereniak, S. J.; DeStefano, M. R.; Buru, C. T.; Li, Z.; Penn, R. L.; Farha, O. K.; Hupp, J. T.; Stein, A.; Lu, C. C. Assembly of Dicobalt and Cobalt–Aluminum Oxide Clusters on Metal–Organic Framework and Nanocast Silica Supports. *Faraday Discuss.* 2017, 201, 287–302. https://doi.org/10.1039/C7FD00055C.
- (10) Zheng, J.; Ye, J.; Ortuño, M. A.; Fulton, J. L.; Gutiérrez, O. Y.; Camaioni, D. M.; Motkuri, R. K.; Li, Z.; Webber, T. E.; Mehdi, B. L.; Browning, N. D.; Penn, R. L.; Farha, O. K.; Hupp, J. T.; Truhlar, D. G.; Cramer, C. J.; Lercher, J. A. Selective Methane Oxidation to Methanol on Cu-Oxo Dimers Stabilized by Zirconia Nodes of an NU-1000 Metal-Organic Framework. *J. Am. Chem. Soc.* 2019, 141 (23), 9292–9304. https://doi.org/10.1021/jacs.9b02902.
- (11) Feng, X.; Song, Y.; Chen, J. S.; Xu, Z.; Dunn, S. J.; Lin, W. Rational Construction of an Artificial Binuclear Copper Monooxygenase in a Metal–Organic Framework. *J. Am. Chem. Soc.* 2021, 143 (2), 1107–1118. https://doi.org/10.1021/jacs.0c11920.
- (12) Baek, J.; Rungtaweevoranit, B.; Pei, X.; Park, M.; Fakra, S. C.; Liu, Y.-S.; Matheu, R.; Alshmimri, S. A.; Alshehri, S.; Trickett, C. A.; Somorjai, G. A.; Yaghi, O. M. Bioinspired Metal–Organic Framework Catalysts for Selective Methane Oxidation to Methanol. J. Am. Chem. Soc. 2018, 140 (51), 18208–18216. https://doi.org/10.1021/jacs.8b11525.
- (13) Pullen, S.; Fei, H.; Orthaber, A.; Cohen, S. M.; Ott, S. Enhanced Photochemical Hydrogen Production by a Molecular Diiron Catalyst Incorporated into a Metal–Organic Framework. *J. Am. Chem. Soc.* **2013**, *135* (45), 16997–17003. https://doi.org/10.1021/ja407176p.
- (14) Wang, Z.; Yeary, P.; Feng, X.; Lin, W. Self-Adaptive Metal-Organic Framework Assembles Di-Iron Active Sites to Mimic Monooxygenases. J. Am. Chem. Soc. 2023, 145 (15), 8647– 8655. https://doi.org/10.1021/jacs.3c01498.
- (15) Ingleson, M. J.; Perez Barrio, J.; Guilbaud, J.-B.; Khimyak, Y. Z.; Rosseinsky, M. J. Framework Functionalisation Triggers Metal Complex Binding. *Chem. Commun.* 2008, No. 23, 2680. https://doi.org/10.1039/b718367d.
- (16) Doonan, C. J.; Morris, W.; Furukawa, H.; Yaghi, O. M. Isoreticular Metalation of Metal–Organic Frameworks. J. Am. Chem. Soc. 2009, 131 (27), 9492–9493. https://doi.org/10.1021/ja903251e.
- (17) Canivet, J.; Aguado, S.; Schuurman, Y.; Farrusseng, D. MOF-Supported Selective Ethylene Dimerization Single-Site

- Catalysts through One-Pot Postsynthetic Modification. *J. Am. Chem. Soc.* **2013**, *135* (11), 4195–4198. https://doi.org/10.1021/ja312120x.
- (18) Rasero-Almansa, A. M.; Corma, A.; Iglesias, M.; Sánchez, F. One-Pot Multifunctional Catalysis with NNN-Pincer Zr-MOF: Zr Base Catalyzed Condensation with Rh-Catalyzed Hydrogenation. *ChemCatChem* 2013, 5 (10), 3092–3100. https://doi.org/10.1002/cctc.201300371.
- (19) Yuan, J.; Fracaroli, A. M.; Klemperer, W. G. Convergent Synthesis of a Metal–Organic Framework Supported Olefin Metathesis Catalyst. *Organometallics* 2016, 35 (12), 2149–2155. https://doi.org/10.1021/acs.organomet.6b00365.
- (20) Lin, Y.; Kong, C.; Chen, L. Amine-Functionalized Metal-Organic Frameworks: Structure, Synthesis and Applications. RSC Adv. 2016, 6 (39), 32598–32614. https://doi.org/10.1039/C6RA01536K.
- (21) Geary, J.; Wong, A. H.; Xiao, D. J. Thermolabile Cross-Linkers for Templating Precise Multicomponent Metal–Organic Framework Pores. J. Am. Chem. Soc. 2021, 143 (27), 10317–10323. https://doi.org/10.1021/jacs.1c04030.
- (22) Protection for the Amino Group. In Greene's Protective Groups in Organic Synthesis; John Wiley & Sons, Ltd, 2006; pp 696– 926. https://doi.org/10.1002/9780470053485.ch7.
- (23) Cohen, S. M. Postsynthetic Methods for the Functionalization of Metal–Organic Frameworks. *Chem. Rev.* **2012**, *112* (2), 970–1000. https://doi.org/10.1021/cr200179u.
- (24) Costa, J. S.; Gamez, P.; Black, C. A.; Roubeau, O.; Teat, S. J.; Reedijk, J. Chemical Modification of a Bridging Ligand Inside a Metal–Organic Framework While Maintaining the 3D Structure. *Eur. J. Inorg. Chem.* **2008**, *2008* (10), 1551–1554. https://doi.org/10.1002/ejic.200800002.
- (25) Dugan, E.; Wang, Z.; Okamura, M.; Medina, A.; Cohen, S. M. Covalent Modification of a Metal–Organic Framework with Isocyanates: Probing Substrate Scope and Reactivity. *Chem. Commun.* 2008, No. 29, 3366. https://doi.org/10.1039/b806150e.
- (26) Taylor-Pashow, K. M. L.; Della Rocca, J.; Xie, Z.; Tran, S.; Lin, W. Postsynthetic Modifications of Iron-Carboxylate Nanoscale Metal—Organic Frameworks for Imaging and Drug Delivery. J. Am. Chem. Soc. 2009, 131 (40), 14261–14263. https://doi.org/10.1021/ja906198y.
- (27) Tanabe, K. K.; Wang, Z.; Cohen, S. M. Systematic Functionalization of a Metal-Organic Framework via a Postsynthetic Modification Approach. J. Am. Chem. Soc. 2008, 130 (26), 8508–8517. https://doi.org/10.1021/ja801848j.
- (28) Ki, C. D.; Oh, C.; Oh, S.-G.; Chang, J. Y. The Use of a Thermally Reversible Bond for Molecular Imprinting of Silica Spheres. J. Am. Chem. Soc. 2002, 124 (50), 14838–14839. https://doi.org/10.1021/ja0277881.
- (29) Bass, J. D.; Katz, A. Thermolytic Synthesis of Imprinted Amines in Bulk Silica. *Chem. Mater.* 2003, 15 (14), 2757– 2763. https://doi.org/10.1021/cm021822t.
- (30) Deshpande, R. K.; Minnaar, J. L.; Telfer, S. G. Thermolabile Groups in Metal-Organic Frameworks: Suppression of Network Interpenetration, Post-Synthetic Cavity Expansion, and Protection of Reactive Functional Groups. *Angew. Chem. Int. Ed.* **2010**, 49 (27), 4598–4602. https://doi.org/10.1002/anie.200905960.
- (31) Lun, D. J.; Waterhouse, G. I. N.; Telfer, S. G. A General Thermolabile Protecting Group Strategy for Organocatalytic Metal–Organic Frameworks. J. Am. Chem. Soc. 2011, 133 (15), 5806–5809. https://doi.org/10.1021/ja202223d.
- (32) Fracaroli, A. M.; Furukawa, H.; Suzuki, M.; Dodd, M.; Okajima, S.; Gándara, F.; Reimer, J. A.; Yaghi, O. M. Metal-Organic Frameworks with Precisely Designed Interior for Carbon Dioxide Capture in the Presence of Water. *J. Am. Chem. Soc.* 2014, 136 (25), 8863–8866. https://doi.org/10.1021/ja503296c.
- (33) Mu, H.; Pan, L.; Song, D.; Li, Y. Neutral Nickel Catalysts for Olefin Homo- and Copolymerization: Relationships between

- Catalyst Structures and Catalytic Properties. *Chem. Rev.* **2015**, *115* (22), 12091–12137. https://doi.org/10.1021/cr500370f.
- (34) McNeill, E.; Ritter, T. 1,4-Functionalization of 1,3-Dienes With Low-Valent Iron Catalysts. Acc. Chem. Res. 2015, 48 (8), 2330–2343. https://doi.org/10.1021/acs.accounts.5b00050.
- (35) Wang, Z.; Liu, Q.; Solan, G. A.; Sun, W.-H. Recent Advances in Ni-Mediated Ethylene Chain Growth: Nimine-Donor Ligand Effects on Catalytic Activity, Thermal Stability and Oligo-/Polymer Structure. *Coordination Chemistry Reviews* 2017, 350, 68–83. https://doi.org/10.1016/j.ccr.2017.06.003.
- (36) Liu, B.; Jie, S.; Bu, Z.; Li, B.-G. Postsynthetic Modification of Mixed-Linker Metal-Organic Frameworks for Ethylene Oligomerization. RSC Adv. 2014, 4 (107), 62343–62346. https://doi.org/10.1039/C4RA10605A.
- (37) Liu, J.; Zhang, X.; Yang, J.; Wang, L. Postsynthetic Modification of IRMOF-3 with a Copper Iminopyridine Complex as Heterogeneous Catalyst for the Synthesis of 2-Aminobenzothiazoles. Applied Organometallic Chemistry 2014, 28 (3), 198–203. https://doi.org/10.1002/aoc.3109.
- (38) Müller, B.; Vahrenkamp, H. Zinc Complexes of Chelating Aldehydes. European Journal of Inorganic Chemistry 1999, 1999
 (1), 137–144. https://doi.org/10.1002/(SICI)1099-0682(199901)1999:1<137::AID-EJIC137>3.0.CO;2-T.
- (39) Lumb, I.; Sran, B. S.; Sood, H.; Arora, D. S.; Hundal, G. Coordination Chemistry of Cu(II), Co(II), Zn(II) and Ag(I) Complexes of Isomeric Pyridine 2- and 4-Carboxamides and Their Biological Activity Evaluation. *Polyhedron* 2017, 127, 153–166. https://doi.org/10.1016/j.poly.2017.01.063.
- (40) Mirica, L. M.; Ottenwaelder, X.; Stack, T. D. P. Structure and Spectroscopy of Copper–Dioxygen Complexes. *Chem. Rev.* 2004, 104 (2), 1013–1046. https://doi.org/10.1021/cr020632z.
- (41) Tshuva, E. Y.; Lippard, S. J. Synthetic Models for Non-Heme Carboxylate-Bridged Diiron Metalloproteins: Strategies and Tactics. *Chem. Rev.* **2004**, *104* (2), 987–1012. https://doi.org/10.1021/cr020622y.
- (42) Eaton, S. S.; Eaton, G. R. Distance Measurements by CW and Pulsed EPR. In *Distance Measurements in Biological Systems* by EPR; Berliner, L. J., Eaton, G. R., Eaton, S. S., Eds.; Biological Magnetic Resonance; Springer US: Boston, MA, 2002; Vol. 19, pp 1–27. https://doi.org/10.1007/0-306-47109-4 1.
- (43) Eaton, G. R.; Eaton, S. S. Measurement of Interspin Distances by EPR. In *Electron Paramagnetic Resonance*; Gilbert, B. C., Ed.; Royal Society of Chemistry: Cambridge, 2008; Vol. 21, pp 59–75. https://doi.org/10.1039/b709149b.
- (44) Eaton, G. R.; Eaton, S. S. Resolved Electron-Electron Spin-Spin Splittings in EPR Spectra. In Spin Labeling; Berliner, L. J., Reuben, J., Eds.; Biological Magnetic Resonance; Springer US: Boston, MA, 1989; Vol. 8, pp 339–397. https://doi.org/10.1007/978-1-4613-0743-3 7.
- (45) Grigoropoulou, G.; Christoforidis, K. C.; Louloudi, M.; Deligiannakis, Y. Structure-Catalytic Function Relationship of SiO2-Immobilized Mononuclear Cu Complexes: An EPR Study. Langmuir 2007, 23 (20), 10407–10418. https://doi.org/10.1021/la700815d.
- (46) Niklas, N.; Alsfasser, R. The Chemistry of Nitrogen Coordinated Tertiary Carboxamides: A Spectroscopic Study on Bis(Picolyl)Amidecopper(II) Complexes. *Dalton Trans.* 2006, No. 26, 3188–3199. https://doi.org/10.1039/B516875A.
- (47) Ghosh, S.; Lawless, M. J.; Brubaker, H. J.; Singewald, K.; Kurpiewski, M. R.; Jen-Jacobson, L.; Saxena, S. Cu2+-Based Distance Measurements by Pulsed EPR Provide Distance Constraints for DNA Backbone Conformations in Solution. *Nucleic Acids Research* 2020, 48 (9), e49. https://doi.org/10.1093/nar/gkaa133.
- (48) Delferro, M.; Marks, T. J. Multinuclear Olefin Polymerization Catalysts. *Chem. Rev.* **2011**, *111* (3), 2450–2485. https://doi.org/10.1021/cr1003634.
- (49) Ngo, H. T.; Liu, X.; Jolliffe, K. A. Anion Recognition and Sensing with Zn(Ii)–Dipicolylamine Complexes. *Chem. Soc. Rev.* 2012, 41 (14), 4928. https://doi.org/10.1039/c2cs35087d.

- (50) Niittymäki, T.; Lönnberg, H. Artificial Ribonucleases. Org. Biomol. Chem. 2006, 4 (1), 15–25. https://doi.org/10.1039/B509022A.

 EasySpin - EPR spectrum simulation. https://easyspin.org/ (ac-
- (51) cessed 2024-03-21).
- Newville, M. Larch: An Analysis Package for XAFS and Related Spectroscopies. *J. Phys.: Conf. Ser.* **2013**, *430*, 012007. https://doi.org/10.1088/1742-6596/430/1/012007. (52)

